Modeling a 3D Eddy Current Problem Using the Weak Formulation of the Convective $\mathbf{A}^*$-ϕ Steady State Method

Jonathan Bird
University of North Carolina – Charlotte
9201 University City Boulevard, Charlotte, NC, 28223
j.bird@uncc.edu

Abstract:

A 3D model of a magnetic rotor both rotating and translationally moving at high-speed over a conductive (non-magnetic) guideway is modeled in steady-state using the convective $\mathbf{A}^*$-ϕ formulation. The formulation is implemented in COMSOL using the weak formulation. The presence of the magnetic rotor (source field) is incorporated into the formulation via the boundary conditions. This type of problem is difficult to model using existing commercial packaged electromagnetic software. However, due to COMSOL weak formulation capabilities such models can be implemented relatively easily. The model is compared with experimental measurements.

Keywords: 3D modeling, eddy currents, magnetic vector potential, weak formulation

1. Introduction

The modeling of devices in which there is two or more degrees of freedom of motion is relatively difficult to simulate. It is especially difficult to determine steady-state conditions when there is high speed translational motion [1]. In this paper a method for modeling a 3D eddy current problem in which both high speed rotation and translational motion is present is outlined. In this example a magnetic rotor is both rotating and translationally moving at high-speed over a conductive (non-magnetic) guideway. The problem is simulated using a steady-state convective $\mathbf{A}^*$-ϕ formulation [1-3]. An illustration of the problem to be modeled is shown in Figure 1. The formulation is implemented in COMSOL using the weak formulation. The presence of the magnetic rotor (source field) is incorporated into the formulation via the boundary conditions [4]. Most existing commercial electromagnetic finite element analysis packages cannot model such an electromagnetic problem. In order to validate the COMSOL model the calculated results are compared with experimental measurements.

2. Use of COMSOL Multiphysics

The weak formulation of COMSOL was utilized. A 2D illustration of the problem domain is shown in Figure 2. The problem formulation within the conducting, Ω_c, and non-conducting regions, Ω_{nc} are discussed in the following four sections.

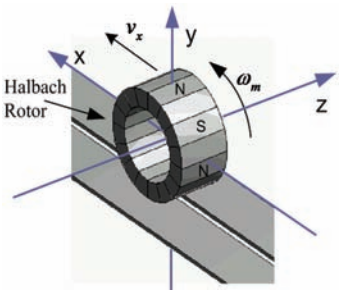

Figure 1. A magnetic rotor both rotating and translationally moving, at high-speed, over a conductive guideway

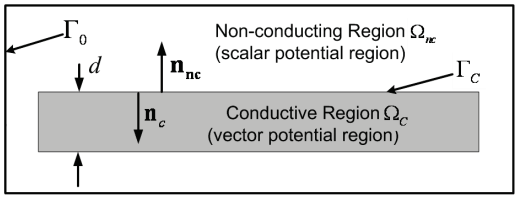

Figure 2. A 2D schematic of the 3D COMSOL Model.

2.1 Conducting Region

If the conductors are assumed to move, rather than the magnets, then the applicable quasi-static Maxwell's equations and vector potential relations within the conductors are [5]

$$\nabla \times \mathbf{E} = -\frac{\partial \mathbf{B}}{\partial t} \quad (1)$$

$$\nabla \times \mathbf{B} = \mu_0 \mathbf{J} \quad (2)$$

$$\nabla \cdot \mathbf{B} = 0 \quad (3)$$

$$\mathbf{J} = \sigma(\mathbf{E} + \mathbf{v} \times \mathbf{B}) \quad (4)$$

$$\mathbf{B} = \nabla \times \mathbf{A} \quad (5)$$

$$\mathbf{E} = -\frac{\partial \mathbf{A}}{\partial t} - \nabla V \tag{6}$$

where σ = guideway conductivity [Sm^{-1}]
$\mathbf{v}$ = velocity [ms^{-1}]
μ_0 = permeability of free space [Hm^{-1}]

If the guideway material is simply connected, linear, homogeneous and composed of non-magnetic material, such as aluminum, then using (1)-(6) and the gauge condition:

$$\nabla \cdot \mathbf{A} = 0 \tag{7}$$

enables the governing guideway equation to be expressed only in terms of the magnetic vector potential [1-3]

$$\nabla^2 \mathbf{A} = \mu_0 \sigma \left(\frac{\partial \mathbf{A}}{\partial t} + (\mathbf{v} \cdot \nabla)\mathbf{A} \right), \text{ in } \Omega_c, \tag{8}$$

The electric scalar potential, *V*, does not need to be modeled when the conductor surface is simply connected [1, 6]. Assuming a steady-state solution can be obtained in which

$$\mathbf{A}(x, y, z, t) = \mathbf{A}(x, y, z) e^{j\omega_e t} \text{ , in } \Omega_c \tag{9}$$

where ω_e is the electric angular velocity, then (8) will become

$$\nabla^2 \mathbf{A} = \mu_0 \sigma \left(j\omega_e \mathbf{A} + v_x \frac{\partial \mathbf{A}}{\partial x} \right), \text{ in } \Omega_c \tag{10}$$

where (10) assumes that the velocity only has an x-component. The three vector potential components in (10) have the same weak form. Using the Galerkin weighted residual procedure (10) can be rewritten, using Green's first identity, as [1]

$$-\int_{\Omega_c} \nabla N_n \cdot \nabla A_n d\Omega_c$$
$$-\mu_0 \sigma \int_{\Omega_c} N_n \left(v_x \frac{\partial A_n}{\partial x} + j\omega_e A_n \right) d\Omega_c$$
$$+\int_{\Gamma_c} N_n (\nabla A_n \cdot \mathbf{n}_c) d\Gamma_c = 0 \tag{11}$$

where $n = x,y,z$ and N_n is the n-component shape function.

2.2 Non-Conducting Region

Within the non-conducting region, in which magnets are present, the total field intensity can be expressed as

$$\mathbf{H} = \frac{\mathbf{B_m}}{\mu_0} - \nabla \phi \text{ , in } \Omega_{nc} \tag{12}$$

Where $\mathbf{B_m}$ is the magnetic rotor complex magnetic flux density and ϕ is the magnetic scalar potential due to the induced guideway currents. If the magnetic material is linear then after taking the divergence of both sides of (12) the formulation for the air region will be

$$\nabla^2 \phi = 0 \text{ , in } \Omega_{nc} \tag{13}$$

Therefore, it is not necessary to explicitly model the rotor's field within the non-conducting region if its effect is accounted for on the conductive regions boundary [7, 8]. After using Green's first identity the weak form of (13) will be

$$\int_{\Omega_{nc}} \nabla \phi \cdot \nabla w_f d\Omega_{nc}$$
$$-\int_{\Gamma_{nc}} w_f \nabla \phi \cdot \mathbf{n}_{nc} d\Gamma_c = 0 \tag{14}$$

where w_f is the weighting function.

2.3 Boundary Conditions

The boundary conditions on the conductive region interface, Γ_c, for the normal and tangential field components are [4]

$$-\mu_0 \nabla \phi \cdot \mathbf{n}_{nc} + \mathbf{B_m} \cdot \mathbf{n}_{nc} = \nabla \times \mathbf{A} \cdot \mathbf{n}_{nc} \tag{15}$$
$$-\mathbf{n}_c \times \mu_0 \nabla \phi + \mathbf{n}_c \times \mathbf{B_m} = \mathbf{n}_c \times \nabla \times \mathbf{A} \tag{16}$$

In addition, in order to ensure the uniqueness of the solution

$$\mathbf{n}_c \cdot \mathbf{A} = 0 \text{ , on } \Gamma_c \tag{17}$$

must also be enforced on the conductive boundaries [6, 7, 9]. The field due to the magnetic rotor and the interfacing between the sub-domains containing the magnetic vector potential and sub-domains containing the scalar potential were incorporated into the weak formulation by modifying the boundary conditions given in (11) and (14). For example, in order to incorporate the scalar potential field and magnetic rotor field into to the conducting region boundary condition (14) becomes

$$\int_{\Gamma_c} w_f \nabla\phi \cdot \mathbf{n}_{nc} d\Gamma_c =$$

$$\int_{\Gamma_c} \frac{w_f}{\mu_0} \left(\mathbf{Bm} - \nabla \times \mathbf{A}\right) \cdot \mathbf{n}_{nc} d\Gamma_c \qquad (18)$$

Similarly, the boundary condition in (11) was replaced by terms that involve the scalar potential and magnetic rotor source field [4]. The 3D source field for the rotor **Bm** was computed semi-analytically using the Biot-Savart law [4].

2.4 Post Processing

The forces on the conducting regions were computed using COMSOL subdomain integration

$$F_x = \frac{1}{2}\mathrm{Re}\left(\int_{\Omega_c} (J_y B_z^* - J_z B_y^*) d\Omega_c\right) \qquad (19)$$

$$F_y = \frac{1}{2}\mathrm{Re}\left(\int_{\Omega_c} (J_x B_z^* - J_z B_x^*) d\Omega_c\right) \qquad (20)$$

$$F_z = \frac{1}{2}\mathrm{Re}\left(\int_{\Omega_c} (J_x B_y^* - J_y B_x^*) d\Omega_c\right) \qquad (21)$$

where, for instance, the J_z current density component is

$$J_z = \sigma(E_z + v_x B_y)$$

$$= -j\omega\sigma A_z + v_x \sigma \left(\frac{\partial A_y}{\partial x} - \frac{\partial A_x}{\partial y}\right) \qquad (22)$$

The star superscript in (19)-(21) denotes conjugation.

5. COMSOL Simulation Results

An example of the iso-surface plot in the non-conducting region due to the induced guideway currents created when the rotor is both rotated and translationally moved is illustrated in Figure 3 while Figure 4 shows the A_z field on the surface of the conductive region when the rotor is rotated over one of the conducting guideway sheets.

5. Experimental Results

In order to validate the COMSOL model the steady-state calculated results were compared with other packaged commercial finite element code in which only rotational and no translational motion was present [4]. In addition, experimental comparisons were made. A summary of the experimental comparison is shown here, further experimental comparisons are provided in [1, 4, 10]. The experimental setup is shown in Figure 5, in which a 1.2m diameter guideway wheel moved below a rotating magnetic rotor. The setup enabled the lift, thrust and lateral forces to be experimentally verified.

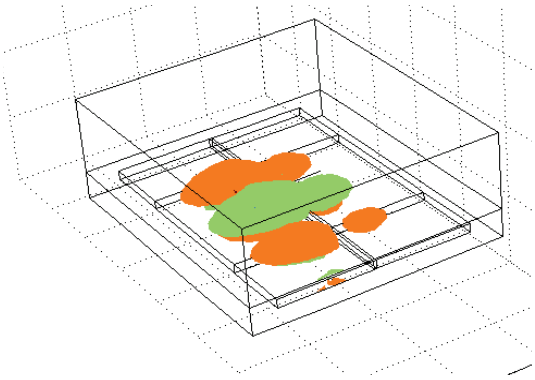

Figure 3. Perspective view of a Bx magnetic flux density iso-surface plot in the non-conducting region due to the induced guideway currents

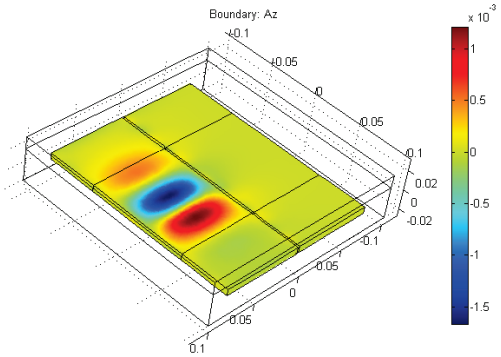

Figure 4. The steady-state boundary coupled A-ϕ finite element model. The A_z field on the surface of the conductive region is shown. The model was written using Matlab and FEMLAB v. 3.1

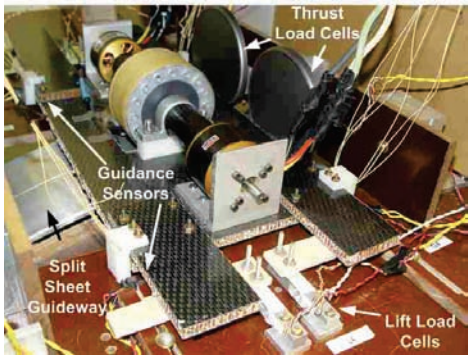

Figure 5. Experimental setup showing magnetic rotor, drive motors, top of the conductive guideway wheel and also load cells.

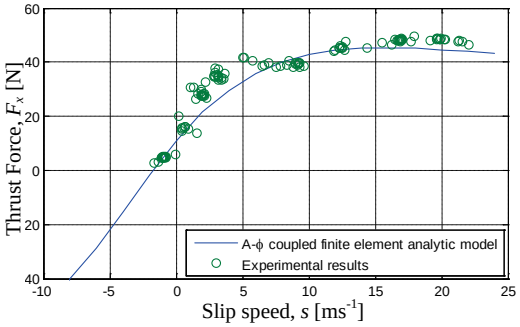

Figure 6 Thrust force comparison for a 15 ms^{-1} translational velocity when EDW over one guideway sheet.

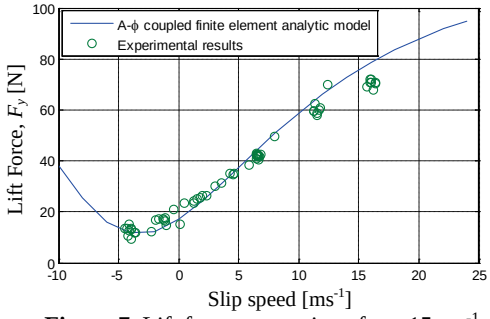

Figure 7 Lift force comparison for a 15 ms^{-1} translational velocity when the rotor is over one guideway sheet.

The forces were measured using load cells. The steady-state measurements were made by keeping the guideway wheel at a constant translational speed, v_x, whilst different rotor slip speeds were obtained by varying the rotor angular velocity, ω_m. A slip speed between the translationally moving conductive guideway and rotating magnetic rotor is therefore present. The slip speed is defined as:

$$s = \omega_m r_o - v_x \qquad (23)$$

where r_o is the outer rotor radius. The parameters used by the experimental setup are shown in Table 1. The effect of the curvature on the experimental guideway wheel has been neglected The COMSOL model's thrust, lift and lateral force were compared with the experimental results. An example of the experimental and finite element comparison when the rotor is translationally moving at 15ms^{-1} and rotating at various speeds (ie: slips) is shown in Figure 6 and Figure 7. Relatively close agreement was obtained. Further comparison are provided in [4].

Table 1 Experimental Parameters

Rotor:	Magnet outer radius, r_o	50 mm± 0.05 mm
	Inner radius, r_i	34.2 mm
	Width, w	50 mm
	Magnet (NdFeB), B_r	1.42T
	Pole pairs, P	4
	Sleeve thickness	2.6 mm ± 0.1 mm
Guideway:	Radius	600 mm ± 0.5 mm
	Conductivity (Al)	2.459×10^7 Sm^{-1}
	Single sheet width	77 mm

	Split sheet gap	2 mm
	Thickness, *d*	6.3mm
	Electrical airgap, *g*	9.5 mm
	'Vehicle mass'	4.8 kg

7. Conclusions

The use of the $\mathbf{A}^*$-ϕ formulation for eddy current analysis significantly reduced the computational burden when compared with using only the magnetic vector potential, **A**, in both the conducting and non-conducting regions. In addition, not explicitly modeling the 3D rotation of the rotor magnets enabled a further reduction in computational burden. The linear nature of this problem enabled a more simplified formation of the $\mathbf{A}^*$-ϕ method in comparison to problems involving non-linear material [2, 7, 9]. The COMSOL model was compared with experimental results and relatively close agreement was obtained.

8. References

1. J. Bird and T. A. Lipo, "A 3D steady-state magnetic charge finite element model of an electrodynamic wheel," *IEEE Trans. Magn.*, **vol. 44**, pp. 253-265, 2008.
2. D. Rodger, P. J. Leonard, et al., "An optimal formulation for 3D moving conductor eddy current problems with smooth rotors," *IEEE Trans. Magn.*, **vol. 26**, pp. 2359-2363, 1990.
3. S. Yamamura, *Theory of Linear Induction Motors*: University of Tokyo Press, 1979.
4. J. Bird and T. A. Lipo, "Modeling the 3-D Rotational and Translational Motion of a Halbach Rotor above a Split-Sheet Guideway," *IEEE Trans. Magn.*, **vol. 45**, pp. 3233-3242, 2009.
5. D. K. Cheng, *Field and Wave Electromagnetics*: Addison-Wesley Publishing, 1989.
6. D. Rodger, T. Karaguler, et al., " A formulation for 3D moving conductor eddy current problems," *IEEE Trans. Magn.*, **vol. Vol. 25**, pp. pp 4147-4149,, 1989.
7. S. Williamson and E. K. C. Chan, "Three-dimensional finite-element formulation for problems involving time-varying fields, relative motion, and magnetic saturation," *IEE Proceedings Part A*, **vol. 140**, pp. 121-130, 1993.
8. D. Rodger and J. F. Eastham, "A formulation for low frequency eddy current solutions," *IEEE Trans. Magn.*, **vol. 19**, pp. 2450-2452, 1983.
9. O. Biró and K. Preis, "On the use of the magnetic vector potential in the finite element analysis of three-dimensional eddy currents," *IEEE Trans. Magn.*, **vol. 25**, pp. 3145-3159, 1989.
10. J. Bird, "An investigation into the use of electrodynamic wheels for high-speed ground transportation," PhD dissertation, Electrical and Computer Engineering, University of Wisconsin-Madison, Madison,WI, 2007